Journal of Power Sources 196 (2011) 9260–9269

Contents lists available at ScienceDirect

Journal of Power Sources

journal homepage: www.elsevier.com/locate/jpowsour

Direct hybrid glucose–oxygen enzymatic fuel cell based on tetrathiafulvalene–tetracyanoquinodimethane charge transfer complex as anodic mediator

Ivan Ivanov[a], Tanja Vidaković-Koch[a,*], Kai Sundmacher[a,b]

[a] Process Systems Engineering, Otto-von-Guericke University Magdeburg, Universitätsplatz 2, 39106 Magdeburg, Germany
[b] Max Planck Institute for Dynamics of Complex Technical Systems, Sandtorstrasse 1, 39106 Magdeburg, Germany

ARTICLE INFO

Article history:
Received 27 May 2011
Received in revised form 14 July 2011
Accepted 16 July 2011
Available online 22 July 2011

Keywords:
Biofuel cell
Glucose oxidation
Glucose oxidase
Glucose crossover
Charge transfer complex

ABSTRACT

TTF–TCNQ has been used for the first time as a mediator in a direct glucose fuel cell operating on gas-phase oxygen. It has been shown that TTF–TCNQ forms highly irregular porous structure, which emphasizes the importance of optimization of mass transport and kinetic resistance in the catalyst layer. Kinetics resistance can be optimized by variation of the mediator and/or enzyme loading, while mass transport resistance mainly by the variation of other structural parameters such as electrode thickness. The optimized anode reached limiting current densities of nearly 400 $\mu A\,cm^{-2}$ in presence of 5 mM glucose under rotation. The enzymatic fuel cell exhibited unexpectedly high OCV values (up to 0.99 V), which were tentatively ascribed to different pH conditions at the anode and the cathode. OCV was influenced by glucose crossover and was decreasing with an increase of glucose concentration or flow rate. Although the performance of the fuel cell is limited by the enzymatic anode, the long-term stability of the fuel cell is mainly influenced by the Pt cathode, while the enzymatic anode has higher stability. The fuel cell delivered power densities up to 120 $\mu W\,cm^{-2}$ in presence of 5 mM glucose, depending on the glucose flow rate.

1. Introduction

Enzymatic fuel cells belong to the group of biofuel cells. The characteristic feature of this fuel cell type is the application of enzymes (biocatalysts) instead of noble metal catalysts. Enzymatic fuel cells are a promising type of fuel cells for niche applications, which benefit from the utilization of enzymes as highly efficient natural catalysts. Advantages of enzymes include activity at mild conditions, lower price and substrate selectivity, which can theoretically enable a membraneless design [1]. The utilization of biocatalysts offers larger number of possible fuels and oxidants as natural substrates of the respective enzymes. The typical fuel in enzymatic biofuel cells is glucose [1] but other sugars, such as fructose [2] and lactose [3], as well as lower aliphatic alcohols, such as ethanol [4] and glycerol [5] have been also used. Contrary to the variety of fuel types, oxygen is almost exclusively used as an oxidant in biofuel cells [1]. Glucose–oxygen enzymatic biofuel cells are promising as power sources for implantable devices [6]. Major drawbacks of these systems are the still low power output and the limited stability.

The enzymes that are employed in this type of fuel cells are called oxidoreductases and catalyze oxidation and reduction processes involving transport of electrons. Oxidoreductases can be coupled with the electrode surface, thus forming enzymatic electrodes, and the electron transfer process can be followed by different electrochemical methods. To construct a biofuel cell system based on redox enzymes, the following points have to be considered: (1) enzyme immobilization; (2) communication between the enzyme and the electrode surface (type of electron transfer); (3) enzyme kinetics; (4) enzymatic electrode architecture; (5) coupling of the electrodes and design of the overall system. The first three points have been extensively studied in the past, mainly regarding the application of these systems as amperometric biosensors. As a result of these activities many preparation methods for enzymatic electrodes can be found in literature. However, only few of them can be employed in systems, where energy production is the main application.

Some examples of mediators in enzymatic electrodes, which have found an application in glucose biofuel cells are ferrocene [7], tetrathiafulvalene (TTF) [8], 8-hydroxyquinoline-5-sulfonic acid (HQS) [9] and Os redox hydrogels [10]. So far, the best performance exhibit Os hydrogels with redox centers attached to a polymer backbone [1]. However, the procedure of synthesizing Os redox hydrogels is usually complicated and involves several steps [11].

* Corresponding author. Tel.: +49 391 6110 319; fax: +49 391 6110 553.
E-mail address: vidakovi@mpi-magdeburg.mpg.de (T. Vidaković-Koch).

0378-7753/$ – see front matter © 2011 Elsevier B.V. All rights reserved.
doi:10.1016/j.jpowsour.2011.07.060

In addition, in respect to the application of enzymatic biofuel cells as implantable power sources, some issues, associated with the toxicity of Os-containing compounds may arise [12]. Another type of mediator, which in our opinion has a great promise for biofuel cell application is the charge transfer complex (CTC) known as organic conductive salt, based on tetrathiafulvalene and tetracyanoquinodimethane (TTF–TCNQ). This complex has been so far mainly used as a mediator in enzymatic electrodes for biosensor applications as outlined in a recent review [13]. Glucose biosensors based on TTF–TCNQ exhibit high current densities, high oxygen tolerance and remarkable stability under continuous operation [14,15]. Khan et al. have shown that glucose biosensors based on TTF–TCNQ can retain up to 40% of their initial response after 100 days of continuous operation and exhibit low sensitivity to the oxygen in normal buffer solutions [14]. However, despite these promising features, TTF–TCNQ anode, to our best knowledge, has not been employed in an enzymatic fuel cell so far. In addition, CTC has several other advantages. Enzymatic electrodes based on TTF–TCNQ do not require complicated modification procedures, in fact they can be prepared as simply as carbon paste electrodes by mixing of the respective components [16]. The TTF–TCNQ salt is commercially available and has high electronic conductivity, which is beneficial for lowering the ohmic resistance within the electrode layer. The morphology of the CTC-crystals can be tuned by variation of the experimental conditions [17]. They can be also prepared in form of nanoparticles [18]. These strategies can be applied to tune the catalytic properties of the CTC and/or to increase the catalytically active surface area. Both TTF and TCNQ have low toxicity, which is attributed to their low solubility in water and physiological fluids [19]. In addition, the catalytic properties of the CTC and the overpotential for glucose oxidation can be further improved by lowering of the redox potentials of its components, e.g. of TTF [20].

To construct an enzymatic electrode for a biofuel cell application the electrode architecture has to be carefully designed and optimized. In the case of enzymes the number of active sites per volume is generally lower than in the case of noble metal electrodes, which issue is crucial in the case of energy-producing systems. This motivates the use of three-dimensional electrode structures instead of monolayer or thin layer configurations [1]. Depending on the type of electron transfer (mediated or direct), a complex network between the enzyme, the mediator and the electron conductive surface has to be established. To tackle experimentally this issue, the influence of the loadings of the respective components in the catalyst layer (composition) and the overall electrode architecture has to be studied, which has not been extensively investigated so far.

The next important aspect is the design of the whole fuel cell system. Little emphasis has been put on this issue in the past and most of the studies have been focused on single electrodes studies. In this work a hybrid biofuel cell device, based on the combination of enzymatic anode and a Pt cathode has been developed. The structure of the cathode comprises the membrane electrode assembly (MEA) design, which has been adopted from the conventional fuel cell technology. The operation with gas-phase oxygen compensates the low solubility of oxygen in aqueous solutions. The combination with a noble metal catalyst electrode allows for testing of the enzymatic electrode performance under fuel cell conditions. Similar strategy has been used both for anodes [21–23] and for cathodes [4,5,24]. Such systems have been usually referred to as biofuel cells, despite of the presence of a non-bio component. The fuel cell device in this study can be used as a platform for investigation of different enzymatic anodes and give additional information about their behavior in a whole fuel cell system when combined with a cathode with "known" catalytic properties.

To summarize, in this paper some aspects regarding the development and design of a hybrid enzymatic fuel cell, such as: (a) the utilization of TTF–TCNQ mediator and the optimization of the three-dimensional electrode structure, (b) anode and cathode coupling and fuel cell design and (c) fuel cell system characterization have been covered.

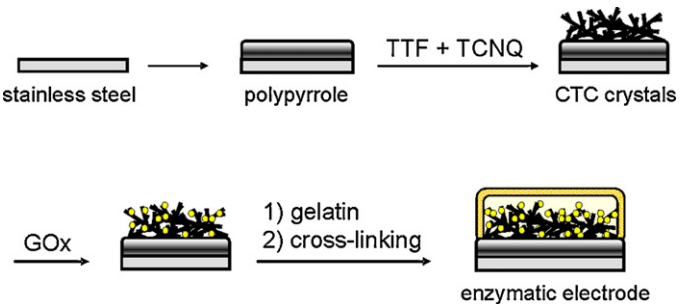

Fig. 1. Schematic presentation of the enzymatic electrode preparation procedure.

2. Materials and methods

2.1. Chemicals and materials

Glucose oxidase (EC 1.1.3.4, GOx) from *Aspergillus niger* was supplied by Fluka. All other chemicals including glucose, TTF, TCNQ and polyvinyl sulfate potassium salt (PVS) as well as tetrahydrofuran (THF) and acetonitrile (ACN) were of analytical reagent grade and purchased from Sigma–Aldrich. Ultrapure water from Millipore was used in all experiments.

Stainless steel was used as a mechanical and electrical support for the preparation of enzymatic electrodes. Discs with a diameter of 11 mm and 1 mm thickness were used in the case of single electrode experiments (three-electrode set-up). The discs were mounted in a sample holder for rotating disc electrode (RDE) with an opening of 8 mm (0.5 cm^2 working area) for the electropolymerization and an opening of 6 mm (0.28 cm^2 working area) for the electrochemical tests. In case of the fuel cell tests (two-electrode set-up), discs with a diameter of 24 mm and 2 mm thickness were used. The surface of the disc was masked by adhesive tape in such a way that a square opening with dimensions of 10 mm × 10 mm (1 cm^{-2} working area) was left exposed.

Nafion 117 was used for the preparation of the MEA. The cathode catalyst ink was based on Platinum Black (Alfa Aesar) and aqueous Nafion solution (Pt:Nafion = 9:1).

2.2. Enzymatic electrode preparation

The enzymatic electrode preparation procedure was similar to the procedure reported by Khan et al. [14] and had several steps, which are schematically presented in Fig. 1. The stainless steel discs were polished with emery paper and degreased with acetone before further modification. In the first step, a polypyrrole film was electrochemically deposited on the stainless steel surface. The electropolymerization was done galvanostatically at a current density of 4 mA cm^{-2} until a charge of 1.2 C cm^{-2} passed. The aqueous monomer solution contained 0.02 M (per monomer molecular weight) PVS and 0.15 M pyrrole. The solution was agitated by the RDE (for 11 mm discs) or a magnetic stirrer (for 24 mm discs). No attempts to exclude oxygen from the system during the electropolymerization were made.

In the next step, CTC crystals were grown directly on the polymer surface. First, TCNQ dissolved in THF was cast several times on the electrode until the desired loading was achieved. After that, TTF dissolved in ACN was applied in several successive steps over the TCNQ layer until TTF loading of slight excess compared to the TCNQ loading was obtained. The electrode was then gently washed with

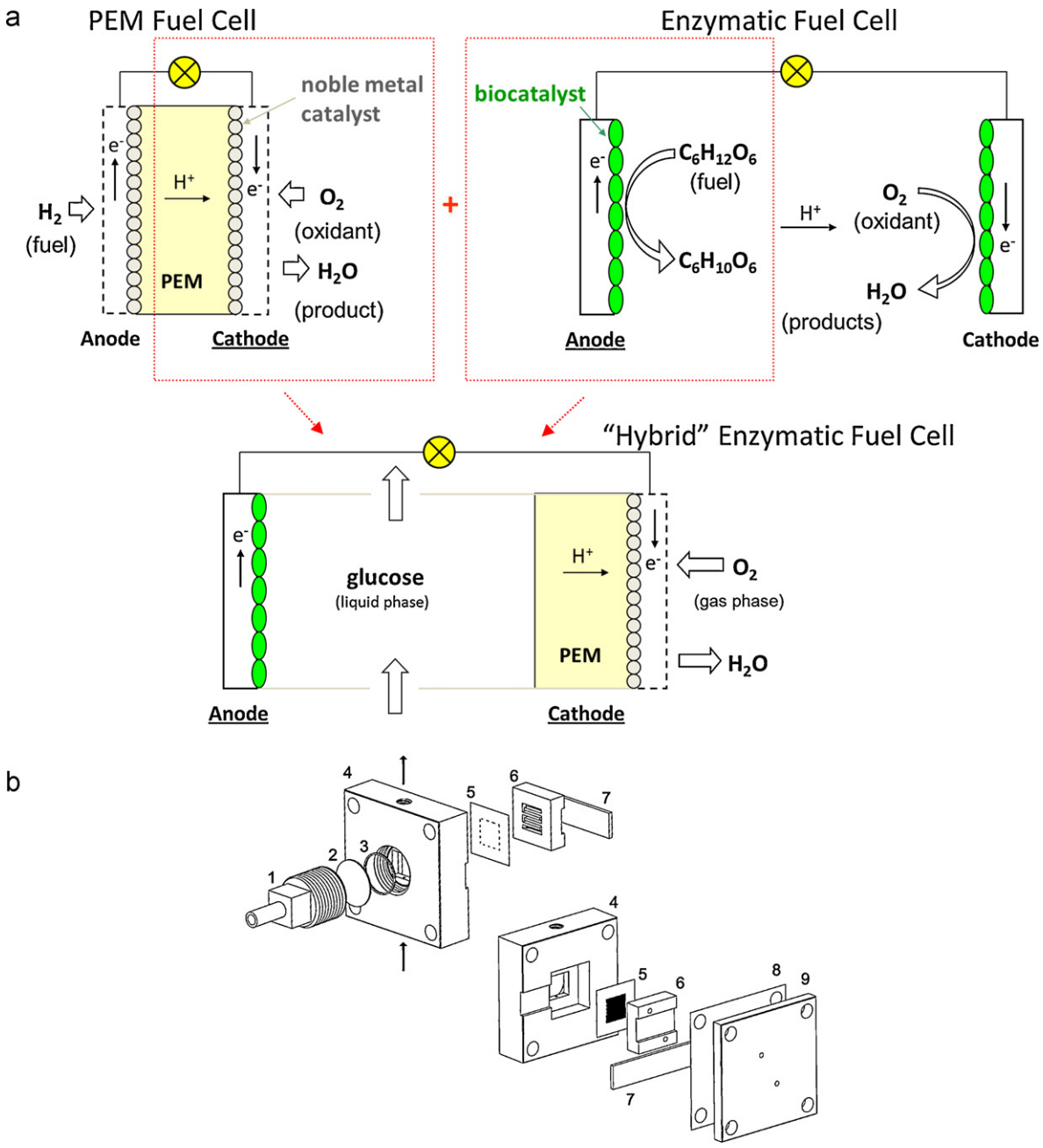

Fig. 2. (a) Schematic presentation of the concept of the hybrid enzymatic fuel cell; (b) an exploded drawing of the fuel cell device with components denoted as follows: 1 – anode current collector, 2 – stainless steel disc with enzymatic catalyst (enzymatic electrode), 3 – O-ring, 4 – cell body, 5 – MEA, 6 – graphite flow-field, 7 – cathode current collector, 8 – PTFE gasket, and 9 – end plate.

ACN in order to remove the unreacted TTF and dried under ambient conditions. After that GOx was adsorbed on the CTC crystals by applying an aliquot of 20 mg ml^{-1} GOx solution in phosphate buffer (pH 7.2) and the electrode was left to dry. Subsequently, the CTC/GOx assembly was covered by an aliquot of gelatin solution (2.5%, w/v in water, incubated for 30 min at 30 °C before use) and dried again.

Finally, the electrode assembly was cross-linked by dipping into a glutaraldehyde solution (5% in water) for 60 s, washed with plenty of water and dried at room temperature. The enzymatic electrodes were kept in plastic bags at −20 °C before use. Cross-sectional scanning electron microscopy (SEM) analysis of the enzymatic electrode assembly was performed by AQura GmbH, Germany using XL30 FEG (FEI Company).

2.3. MEA preparation and fuel cell construction

The MEA's were prepared in-house by spray-painting of the catalyst ink on one of the sides of a Nafion membrane until a loading of approximately 5 mg cm^{-2} was achieved. The projected catalyst area had a square shape with dimensions 10 mm × 10 mm (1 cm^{-2} working area, corresponding to the anode working area). After that the MEA's were sintered at 135 °C for 30 min and left to cool down.

The concept of the hybrid enzymatic fuel cell presented in this study, which is based on the coupling of a bioanode and a Pt cathode is shown schematically in Fig. 2a. It should be noted that the term "hybrid" when referred to a fuel cell, is mainly associated with the combination of two power sources with different operational principles (e.g. fuel cell and battery). However, this term can be

also used to denote the different nature of catalysts (e.g. biological catalyst at the anode and an inorganic catalyst at the cathode as in the present case) as discussed in [1]. Three-dimensional drawing of the resulting device and its components is shown in Fig. 2b. The cell body was transparent and made out of Makrolon (Bayer). The stainless steel disc covered with anodic catalyst was fixed to the cell body by the anode current collector and sealed by an O-ring. The MEA was placed on the opposite side of the cell body with the bare side of the membrane facing the anodic compartment. A graphite plate with a flow-field was used for gas distribution and a gold-coated copper plate served as a cathode current collector. The cathode components were clamped together and sealed by a polytetrafluoroethylene (PTFE) gasket and an end plate, which ensured leak tightness and good electrical contact in the whole assembly. In some cases cellophane P00 (Innovia Films) was used as a separator between the MEA and the anodic compartment (not shown in Fig. 2b).

The fuel cell was mounted vertically in a holder in such a way that the fuel solution was flowing upwards through the cell (see arrows indicating flow direction in Fig. 2b), whereby the perfusion flow was sustained by a peristaltic pump. The cell was connected to a fuel reservoir, equipped with a temperature control and gas supplies to allow for operation with nitrogen- or oxygen-saturated media. The fuel solution was 0.1 M phosphate buffer with different glucose concentrations. The cathode was fed with dry oxygen at a flow rate of ca. 500 ml min^{-1}.

2.4. Electrochemical experiments

Single electrode experiments were carried out in a conventional double-jacketed Pyrex electrochemical cell (Radiometer Analytical). The RDE was used as a working electrode, platinum wire as a counter electrode, and saturated calomel electrode (SCE) as a reference electrode. The experimental solutions were saturated with nitrogen or oxygen. Electrochemical single electrode and fuel cell experiments were performed by a computer controlled potentiostat PGSTAT302 (Eco Chemie/Autolab). In case of fuel cell experiments, before measurements, the cell was left to equilibrate with constant flow of reactants until a stable open circuit voltage (OCV) value was obtained. The data for polarization curves have been extracted from transient measurements after 2 min at constant voltage.

3. Results and discussion

3.1. Optimization of the electrode architecture

3.1.1. Enzymatic electrode characterization with SEM

A SEM image of the enzymatic electrode assembly cross section, peeled off from the stainless steel support, is shown in Fig. 3. Three layers can be clearly distinguished and the thickness of every layer has been estimated from the micrograph as follows: 2 μm polypyrrole layer, 60 μm catalyst layer, composed of CTC crystals with adsorbed GOx, and 5 μm gelatin layer. As can be seen in Fig. 3 the catalyst layer of the enzymatic electrode is characterized by randomly distributed CTC bundles and cavities, forming a highly irregular porous structure, which serves as a matrix for enzyme immobilization. According to previous reports, this matrix was described as a standing highly branched tree-like structure emerging from the polymer layer with a size of 40–50 μm [14,15]. This presentation seems to be unrealistic taking into account the present results for electrodes with similar CTC loading. SEM observations in the present case did not indicate CTC crystals penetrating the polypyrrole layer as reported in [15] or structures, vertically standing on the electrode surface [14]. Another important observation is that unlike the previously reported presentation of gelatin, penetrating the CTC crystals and stabilizing the respective structure, the gelatin layer in the present case penetrates little in the catalyst layer and forms a well-defined membrane on top. This will influence the transport properties of the catalyst layer, which has significance especially for further modeling of the enzymatic electrode.

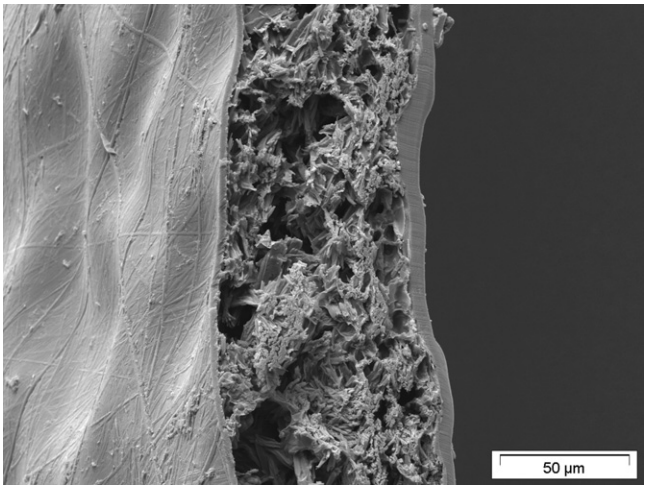

Fig. 3. A SEM image of the enzymatic electrode cross-sectional view.

3.1.2. Cyclic voltammetry characterization of the enzymatic electrodes

The electrochemical behavior of the enzymatic electrode has been studied between −0.2 and 0.2 V vs. SCE in 0.1 M phosphate buffer (pH 7.2), since this potential region is regarded as “stable”, where no CTC decomposition occurs [25]. Representative cyclic voltammograms of the bioanode in presence of different glucose concentrations are shown in Fig. 4a. As can be seen, despite the low sweep rate, large capacitive currents, exceeding the reaction currents, are observed. According to experiments with electrodes lacking polypyrrole, the pronounced capacitive behavior should be ascribed to the underlying polymer surface and not to the high surface area of the CTC crystals or to the underlying stainless steel support, as shown in Fig. 4b (note the axis scales). Similar voltammetric behavior exhibiting large capacitive currents has been reported by Pauliukaite et al. in the case of a TTF–TCNQ-based biosensor for determination of glutamate [16]. The base voltammograms in absence of glucose indicate some oxidative process occurring at the stainless steel surface at more positive potentials (Fig. 4b) but the associated currents are negligible compared to the currents due to glucose oxidation. As can be seen in Fig. 4a the bioanode exhibits activity for glucose oxidation and the currents increase with substrate concentration. Maximum current in presence of 5 mM glucose reaches ca. 110 μA (corrected for the background current), which corresponds to nearly 400 μA cm^{-2} current density. The open circuit potential of the enzymatic electrodes after equilibration in the electrochemical cell under rotation in presence of glucose was typically around −0.2 V vs. SCE, while as can be seen in Fig. 4a the oxidation onset observed in the positive scans is at ca. −0.1 V vs. SCE. In general, the onset potential for the glucose oxidation reaction is mainly related to the type of mediator used in the system, which can be immobilized on the electrode or dissolved in the electrolyte. As it has been recently discussed, electrode systems with dissolved mediators are not appropriate for biofuel cell applications [1]. Some typical values for the glucose oxidation onset potentials in the case of enzymatic anodes with immobilized enzymes and mediators, which have been successfully employed in biofuel cells, are ca. 0 V vs. SCE in presence of

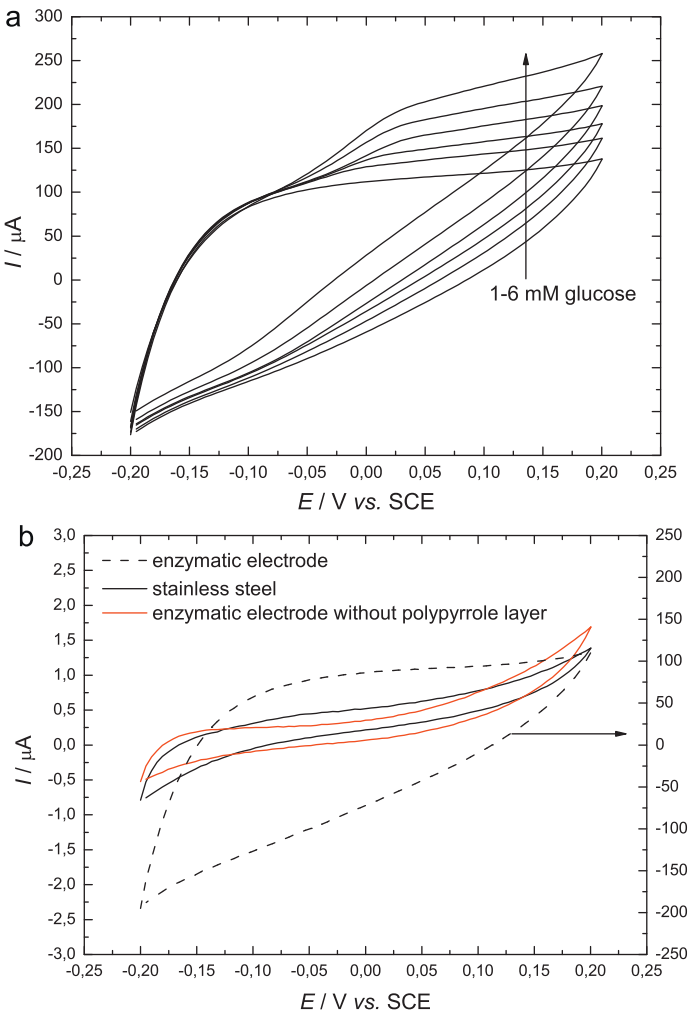

Fig. 4. Cyclic voltammograms of (a) the enzymatic electrode in presence of different glucose concentrations (1–6 mM); (b) the enzymatic electrode, stainless steel support and enzymatic electrode lacking the polypyrrole layer in absence of glucose. Conditions: 0.1 M phosphate buffer, pH 7.2, 37 °C, 400 rpm, N_2 atmosphere, sweep rate: 5 mV s^{-1}.

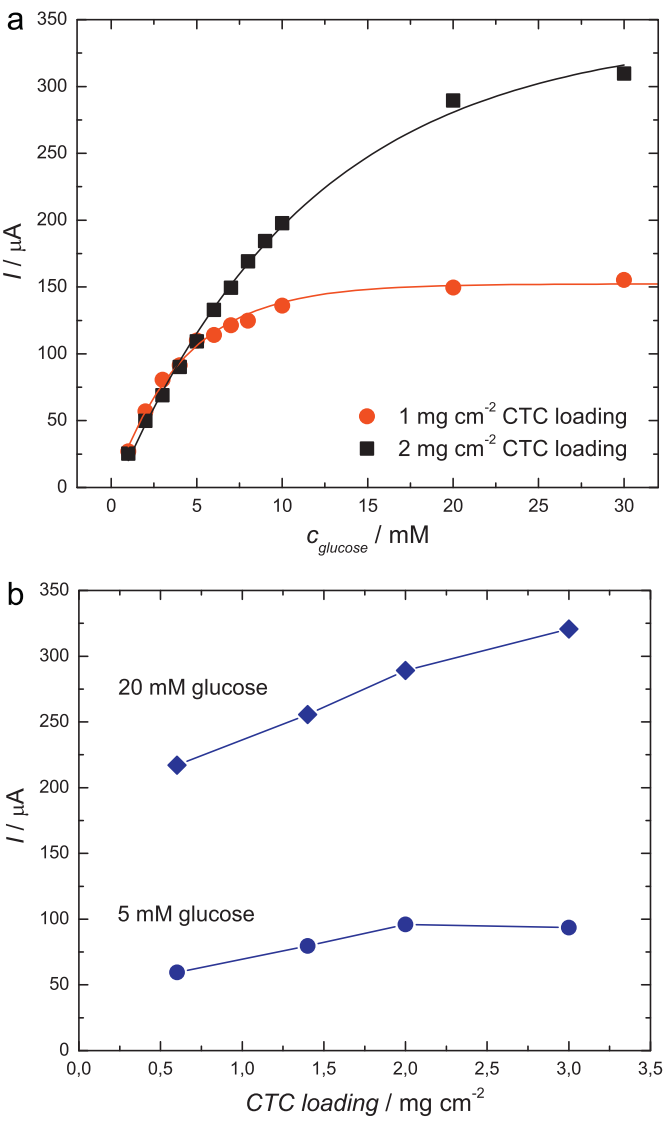

Fig. 5. (a) Concentration dependence of the current at 0.2 V vs. SCE (corrected for the background current) for two enzymatic electrodes with different CTC loadings; (b) dependence of the current at 0.2 V vs. SCE (corrected for the background current) in presence of 5 mM and 20 mM glucose on the CTC loading. Data extracted from cyclic voltammetry. Conditions for the cyclic voltammetry experiments similar as in Fig. 4.

60 mM glucose for a ferrocene-based mediator [26], between ca. −0.1 and 0 V vs. SCE in presence of 20 mM glucose for electrodes based on TTF [27,28] and ca. −0.4 V vs. SCE at 15 mM glucose for an Os hydrogel [11]. The CTC-based electrode in the present work shows 100 mV more negative onset potential than the electrodes based on ferrocene and similar value to TTF, while it is clearly outreached by the Os-based mediator. However, as already discussed, the present system offers some other advantages.

3.1.3. *Influence of the CTC, GOx and gelatin loadings*

As already shown in Fig. 3 the catalyst layer has a highly irregular porous structure and it can be anticipated that the enzyme distribution within this layer will have significant effect on the activity of the enzymatic electrode. To optimize the performance of the electrode, the ratio between CTC and GOx has been varied in a systematic way. In addition the influence of the thickness of the gelatin layer has been also checked.

The concentration dependencies of the current at 0.2 V vs. SCE (corrected for the background current) of two enzymatic electrodes with different CTC loadings are shown in Fig. 5a. The CTC loading was found to have a minor influence at lower glucose concentrations and higher impact at higher glucose concentrations, shifting the currents at 30 mM glucose from ca. 150 µA for 1 mg cm^{-2} CTC to ca. 310 µA for 2 mg cm^{-2} CTC. Also, the linear region in the concentration dependence was extended with an increase of the loading.

The influence of the CTC loading has been additionally investigated and the dependencies of the limiting currents at 5 and 20 mM glucose are presented in Fig. 5b. 5 mM glucose has been chosen as the operational concentration of interest (normal glucose concentration in the human body) and 20 mM has been chosen as a concentration, close to saturation. As can be seen, at 5 mM a CTC loading, higher than 2 mg cm^{-2} does not influence the current output anymore, while at 20 mM the current increases in the whole investigated range. Based on the current results, 2 mg cm^{-2} has been chosen as the optimum CTC loading for further tests in presence of 5 mM glucose. Similar investigation of the influence of CTC loading has been presented in a previous work, where the authors reported an optimum value of about 2 mg cm^{-2} for the CTC loading [14]. It should be noted that in the latter case the electrode modification procedure involved adsorption of the enzyme on the CTC crystals and subsequent removal of the excess enzyme solution. This implies a combined effect of both loadings, whereby the

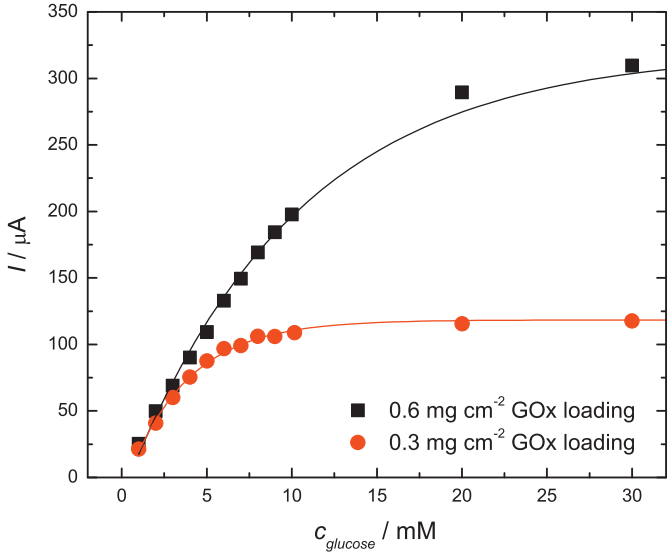

Fig. 6. Concentration dependence of the current at 0.2 V vs. SCE (corrected for the background current) for two enzymatic electrodes with different GOx loadings. Data extracted from cyclic voltammetry. Conditions for the cyclic voltammetry experiments similar as in Fig. 4.

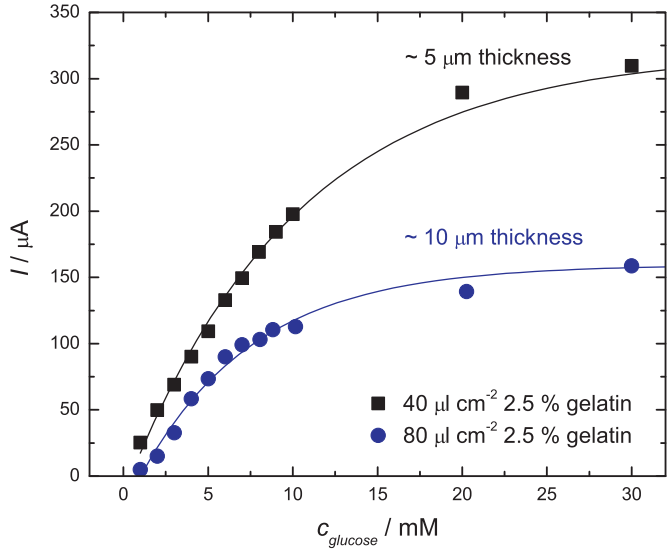

Fig. 7. Concentration dependence of the current at 0.2 V vs. SCE (corrected for the background current) for two enzymatic electrodes with different gelatin loadings. Data extracted from cyclic voltammetry. Conditions for the cyclic voltammetry experiments similar as in Fig. 4.

amount of adsorbed GOx increases with the CTC loading (shown by spectrophotometric measurements) and restricts the discrimination between both effects. In the latter work the authors reported also mechanical instability of the crystal structure by loadings higher than 2 mg cm^{-2}, which was not observed in the present case.

The influence of the GOx loading on the anode performance in the present study has been tested at constant CTC loading. The effect is similar to the effect observed in the case of CTC (Fig. 6). Decreasing the GOx loading twice suppresses the currents at higher glucose concentrations, decreases the linear region and shifts the saturation concentration to lower values (ca. 10 mM).

In a similar manner, the gelatin loading has been varied by keeping the other two structural parameters constant. Doubling of the gelatin loading decreases the currents as can be seen in Fig. 7. The current decrease is more pronounced at higher glucose concentrations but the relative current ratio is approximately 60% in the whole concentration range. This effect has been ascribed to limited mass transport of glucose through the gelatin layer. Such change in the concentration dependence with an increase of the thickness was reported also in the case of polysiloxane membranes [29].

The influence of the investigated structural parameters on the bioelectrode response can be interpreted in terms of the mechanism of enzymatic glucose oxidation. Previous studies regarding electrode with a similar architecture assumed direct regeneration of the reduced enzyme at the CTC surface and discussed the influence of CTC loading in a rather phenomenological way [14]. Contrary to the latter case, the effects of the investigated structural parameters are discussed in terms of the assumed reaction mechanism. If one considers a mediated electron transfer, the overall oxidation mechanism will be governed by the following equations:

$$S_{bulk} \xrightarrow{diffusion} S_{surface}$$

$$S_{surface} + E_{ox} \underset{k_{-1}}{\overset{k_1}{\longleftrightarrow}} ES \xrightarrow{k_{cat}} E_{red} + P$$

$$E_{red} + M_{ox} \xrightarrow{k_2} E_{ox} + M_{red}$$

$$M_{red} \xrightarrow{k_3} M_{ox} + ne^-$$

where S is the substrate (glucose), E is the enzyme (GOx), ES is enzyme-substrate complex, P is the product (gluconolactone) and M is the mediator. The oxidized and reduced forms of enzyme and mediator are denoted by the respective index.

According to the literature both TTF and TCNQ can act as mediators for GOx [8,30]. The unique properties of the CTC, including high electrical conductivity and the absence of a redox peak in the catalytically relevant potential region have obstructed the unambiguous clarification of the electron transfer mechanism. Recently, the concept of alternating (involving different species) mediated electron transfer, depending on the applied potential, has been proposed ([13] and reference therein). In general it should be noted that, although important for the sake of better understanding, at this stage the exact identification of the mediator does not influence the conclusions that can be drawn from the experiments shown above.

The sensitivity of the electrode response in the limiting current region on all three investigated parameters suggests a mixed reaction-mass transfer limitation. The change of the gelatin loading effectively changes the thickness of the membrane layer, which increases the mass transfer resistance for glucose transport and decreases the glucose concentration at the electrode surface ($S_{surface}$).

The increase of enzyme loading will increase the rate of the reaction between glucose and enzyme. It can be easily anticipated, even in terms of simple Michelis–Menten kinetics that the increase of the enzyme loading will increase the slope of the concentration dependence in the linear region ($K_M \gg [S]$) and it will change the value of the current response in the limited region ($K_M \ll [S]$), which has been qualitatively observed in the present study (see Fig. 6). The increase of the CTC loading will effectively increase the concentration of the mediator in the catalyst layer, which will lead to increase in the electrode response. At lower substrate concentrations the change of CTC loading has less influence, which means that under these conditions the total reaction rate is not dominated by the enzyme–mediator reaction. At higher substrate concentrations (e.g. 20 mM) the increase of the CTC loading produces the continuous increase of the electrode response.

For further studies in the hybrid fuel cell, the following values for the investigated structural parameters have been used: 2 mg cm^{-2} CTC loading, 0.6 mg cm^{-2} GOx loading and 40 μl cm^{-2} 2.5% gelatin solution, which corresponds to ca. 5 μm thickness.

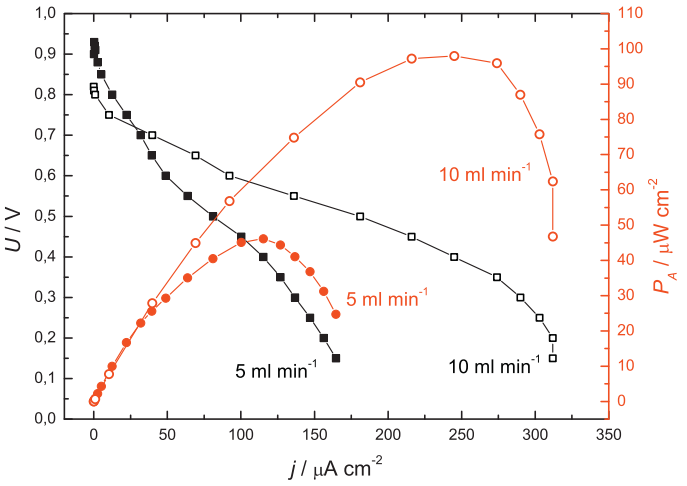

Fig. 8. Polarization (black squares) and power curves (red circles) of the hybrid fuel cell at glucose flow rates of 5 ml min^{-1} (full symbols) and 10 ml min^{-1} (empty symbols). Conditions: anode 5 mM glucose in 0.1 M phosphate buffer, pH 7.2, 37 °C, N_2 atmosphere; cathode 500 ml min^{-1} dry oxygen flow rate. Data extracted from transient measurements after 2 min. (For interpretation of the references to color in this figure legend, the reader is referred to the web version of the article.)

3.2. Performance of the hybrid enzymatic fuel cell

The enzymatic fuel cell device, presented in this study comprises a parallel plate design (see Fig. 2a, b). The bioanode operates in liquid phase and the flow-through design of the anodic chamber allows for perfusion of the fuel solution. The continuous flow diminishes substrate depletion and product accumulation and allows for mass transport investigations of the bioanode under fuel cell conditions. In case of a batch operation or when analysis of the oxidation products is required, the flow can be stopped and the anodic chamber can be isolated by closing the inlet and outlet valves.

The cathode operates in gas phase, which allows for overcoming of the limitations associated with the low oxygen solubility in aqueous solutions [31]. The use of pure oxygen instead of air and the high flow rate (500 ml min^{-1}) should eliminate oxygen concentration effects along the flow field channels. The oxygen gas was not humidified due to the fact that the one side of the membrane is in contact with aqueous solution and should be sufficiently hydrated. The high platinum loading (5 mg cm^{-2}) should ensure high cathode performance as it was shown by Reshetenko et al. [32], who studied the influence of cathode optimization on the performance of a direct methanol fuel cell (DMFC).

Polarization and power curves of the enzymatic fuel cell at two different glucose flow rates are shown in Fig. 8. The polarization curve at 5 ml min^{-1} flow rate exhibits a small activation region and an OCV of 0.94 V. Different OCV values for glucose–oxygen biofuel cells have been presented in the literature. For example, 0.55 V was reported for a similar flow-through fuel cell with enzymatic anode mediated by dissolved benzoquinone and a Pt cathode [33] or 0.8 V for a non-enzymatic direct glucose fuel cell based on Pt catalysts, which employed also a MEA design [34]. High OCV values (around 1 V) have been demonstrated in the case of glucose–oxygen enzymatic biofuel cells based on Os redox hydrogels [35,36]. The theoretical cell voltage for glucose oxidation to gluconolactone in presence of gas-phase oxygen under standard conditions, calculated according to [37] and assuming ionic strength of 0.25 M is 1.18 V, which corresponds to the value calculated in [35]. If conditions deviate from standard conditions as in the present case (5 mM glucose concentration and not defined concentration of gluconolactone, which is consumed in a following hydrolysis reaction) even higher theoretical cell voltage can be expected according to the Nernst equation. Although reasonable from a thermodynamic point of view, the value of 0.94 V is unexpectedly high, compared to the typical performance of similar biofuel cells.

The OCV in a fuel cell is influenced by the open circuit potentials of the anode and the cathode. As it was already mentioned, the open circuit potential of the anode in the present case is around −0.2 vs. SCE. On the other side, control experiments with Pt black-modified electrodes (not shown here) revealed current onset of the oxygen reduction at about 0.3 V vs. SCE in phosphate buffer, which was in accordance with the literature values for Pt nanoparticles on multi-walled carbon nanotubes (MWCNT's) (ca. 0.26 V vs. SCE) [38]. According to these half-cell experiments one can expect much lower OCV. The high values obtained in the present study can be tentatively explained by the specific architecture of the fuel cell, namely the enzymatic electrode is in contact with buffer, while the Pt cathode is in contact with Nafion. This implies pH difference between the electrodes. In control experiments the Pt black cathodes in 0.1 M sulfuric acid (not shown) revealed reduction onset at approximately 0.7 V vs. SCE, which was similar to the value for Pt nanoparticles on MWCNT's in 0.1 M perchloric acid [39]. Furthermore, the oxygen reduction kinetics is significantly enhanced at the Pt/Nafion interface since Nafion is a superacid (due to the highly acidic protons attached to the sulfonate sites in the polymer structure) and exhibits negligible anion adsorption effects, in addition to high oxygen solubility [40], which implies even more positive onset potential for the Pt cathode than the one observed in the case of sulfuric acid. In light of the discussion above, the measured OCV values can be expected in the present setup. Regarding the value of 0.55 V, reported for a similar hybrid setup [33], the difference can be possibly attributed to the different fuel cell architecture, the higher glucose concentration and the different mediator. Higher glucose concentration is expected to increase the glucose crossover and consequently to decrease OCV, which will be discussed below.

In addition to the activation region, observed in Fig. 8, the mass transport and resistance limitation regions in the polarization curve can be also distinguished. The current values obtained in the present setup suggest that the fuel cell is limited by the enzymatic anode since the Pt cathode can easily reach the mA range under similar conditions, e.g. in a DMFC [41]. The fuel cell exhibits maximum power density of about 45 μW cm^{-2} at 5 ml min^{-1} glucose flow rate. Increasing the flow rate to 10 ml min^{-1} decreases the OCV to 0.82 V and changes the shape of the polarization curve. The region of ohmic polarization is significantly extended and the mass transport limitation can be clearly identified at current densities around 300 μA cm^{-2} (see Fig. 8). The decrease in OCV at higher flow rate can be attributed to crossover of glucose, which can be oxidized at the cathode, creating a mixed potential. Increase in flow rate is expected to enhance the mass transport of glucose at the anode but also to increase the rate of crossover. Such phenomenon has been also demonstrated in a recent study, where the influence of operational parameters such as fuel concentration and flow rate on the performance of a DMFC has been investigated [41]. The higher flow rate in the present case resulted in an improved overall performance of the fuel cell, raising the maximum power output to nearly 100 μW cm^{-2} at 0.4 V.

The performance of the fuel cell presented in this study is somewhat superior compared to other hybrid biofuel cells employing Pt cathodes, although a straightforward comparison is difficult due to the difference in experimental conditions as outlined in [1]. For instance, a fuel cell with similar MEA architecture, which delivered around 45 μW cm^{-2} at 100 mM glucose, was reported by Tamaki et al. [42]. The anode was based on GOx and a ferrocene-modified polymer, which redox potential resulted in lower OCV and moderate output despite the high fuel concentration. Another compartmentalized fuel cell, which utilized GOx and dissolved

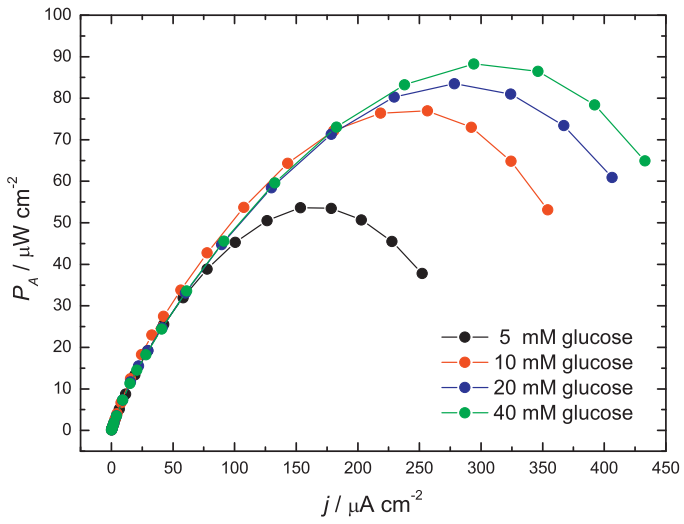

Fig. 9. Power curves of the hybrid fuel cell with separator in presence of different glucose concentrations. Conditions: anode 5 ml min^{-1} glucose flow rate, 0.1 M phosphate buffer, pH 7.2, 37 °C, N_2 atmosphere; cathode 500 ml min^{-1} dry oxygen flow rate. Data extracted from transient measurements after 2 min.

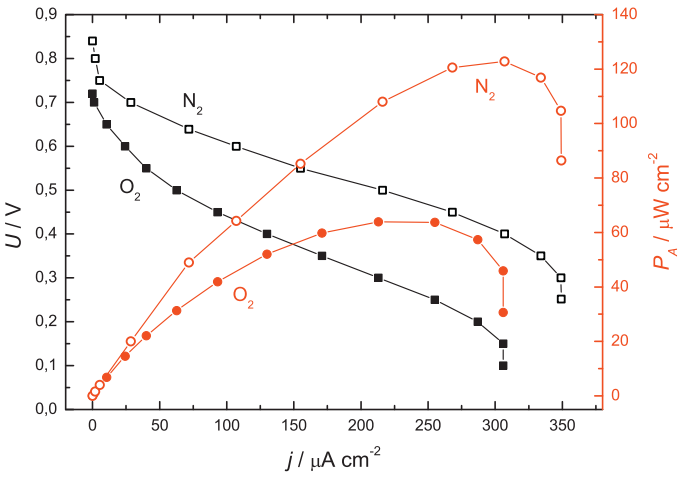

Fig. 10. Polarization (black squares) and power curves (red circles) of the hybrid fuel cell in presence of nitrogen- (empty symbols) and oxygen-saturated (full symbols) glucose solution. Conditions: anode 20 ml min^{-1} flow rate, 5 mM glucose in 0.1 M phosphate buffer, pH 7.2, 37 °C; cathode 500 ml min^{-1} dry oxygen flow rate. Data extracted from transient measurements after 2 min. (For interpretation of the references to color in this figure legend, the reader is referred to the web version of the article.)

benzoquinone as mediator generated similar output (42 μW cm^{-2}) also at 100 mM glucose [43].

In another study, highly efficient bioelectrodes based on Os redox hydrogels, single-walled carbon nanotubes (SWCNT's) and CDH were tested in a model membraneless configuration together with a Pt black cathode and the resulting maximum power density was 157 μW cm^{-2} in presence of 100 mM glucose.

The performance of the biofuel cell presented in this study is also comparable to the performance of biofuel cells incorporating enzymatic cathodes. For instance, a very recent study reported high current density glucose oxidation anodes based on GOx and a ferrocene-modified polymer, which generated limiting current densities of about 2 mA cm^{-2} at 0.3 V vs. SCE and ca. 60 mM glucose [26]. The bioanodes were coupled with Os-mediated laccase cathodes and the resulting biofuel cell generated 56 μW cm^{-2} with a stationary cathode and 146 μW cm^{-2} under rotation. In respect to operation at low glucose concentrations (5 mM), a notable example is the configuration based on Os redox hydrogels, which generated 280 μW cm^{-2} and was reported as the highest power biofuel cell at the lowest concentration [44]. However, this high performance in the latter case was achieved by the use of GOx from another source (*Penicillium pinophilum*) and operation at pH 5. For comparison, when GOx from *Aspergillus niger* was used, the biofuel cell generated only 90 μW cm^{-2} under the same conditions. In addition, it should be noted that the respective electrodes were 2 cm long carbon fibers with a diameter of 7 μm, which size and geometry significantly enhance mass transport conditions.

3.3. Influence of operational parameters on the performance

As already shown the glucose crossover can decrease the performance of the fuel cell. To overcome this effect, a cellophane separator has been introduced in the experiments with higher glucose concentrations. The utilization of separator resulted in an improved performance of the hybrid enzymatic fuel and increased the maximum power density. Power curves of the enzymatic fuel cell with a separator in presence of different glucose concentrations are shown in Fig. 9. The maximum power density is shifted from ca. 55 μW cm^{-2} at 5 mM glucose to ca. 90 μW cm^{-2} at 40 mM glucose. The increase is not linear, which fits well to the observations in single electrode experiments. The OCV values decreased by increasing the glucose concentration from ca. 0.99 V at 5 mM glucose to ca. 0.94 V at 40 mM glucose, which was ascribed to glucose crossover to the cathode. Similar decrease of OCV by increasing fuel concentration was demonstrated by Chen et al. in the case of a DMFC [41].

An important prerequisite for the utilization of enzymatic anodes in a membraneless fuel cell design is their oxygen tolerance. This concern is especially relevant in the case of enzymatic systems based on GOx since oxygen is believed to be the enzyme's natural electron acceptor and would compete for the electrons released by the oxidation [1]. Polarization and power curves of the hybrid enzymatic fuel cell without separator fed with nitrogen- and oxygen-saturated glucose solutions are shown in Fig. 10. As can be seen from the graph the presence of oxygen in the fuel solution decreases the overall fuel cell performance in the whole investigated range so the shape of the polarization curve remains qualitatively the same. The OCV drops by 120 mV and the maximum power density decreases from ca. 120 μW cm^{-2} to ca. 65 μW cm^{-2} in presence of oxygen. This observation is in accordance with single electrode experiments, in which a similar rate of performance reduction has been observed (not shown here). The decrease in current densities is associated with the reduced number of electrons, which instead of being transported through the mediator to the electrode surface are consumed by oxygen. The OCV drop on the other side could be the consequence of the generation of a mixed potential at the anode in presence of oxygen.

3.4. "Long-term" stability of the hybrid fuel cell

The stability of the hybrid fuel cell has been investigated by constant polarization at 0.5 V at two different glucose flow rates. For comparison, the chronoamperometric response of the enzymatic anode, polarized at 0.05 V vs. SCE under forced convection conditions has been also shown. As can be seen in Fig. 11a, the anode and the fuel cell at lower flow rate exhibit similar rather stable behavior. Increase in flow rate results in higher currents due to enhanced glucose transport to the enzymatic electrode but with the expense of reduced stability.

When the time scale at the higher flow rate was extended to 24 h, the current decayed to 1 μA cm^{-2} as shown in Fig. 11b. Such a pronounced loss of activity during long-term operation can be due to several reasons, including anode and cathode deactivation or a

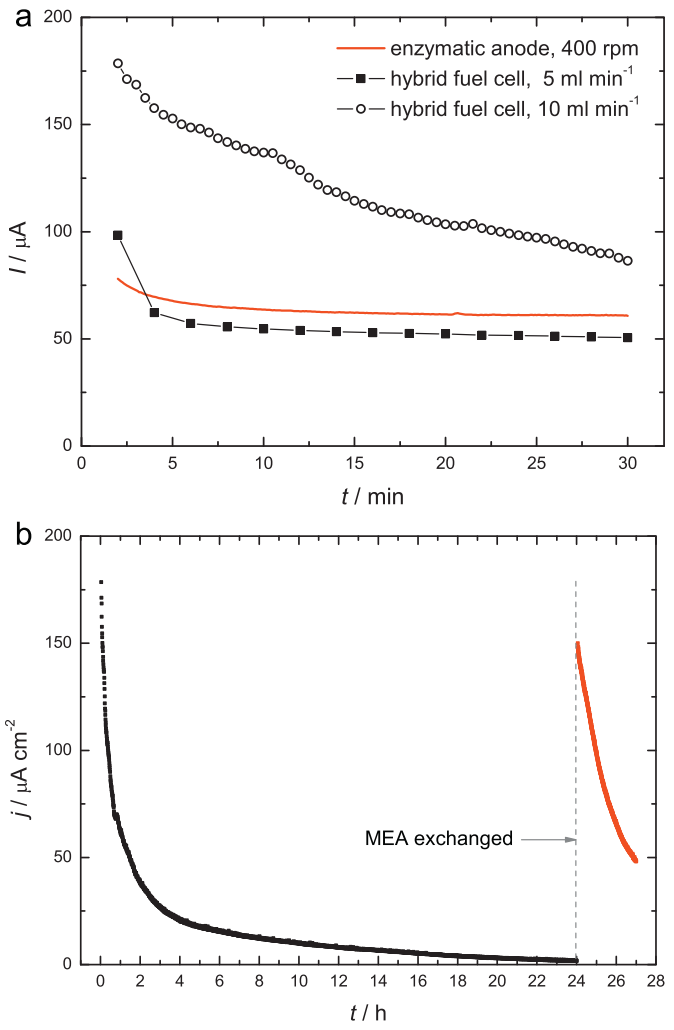

Fig. 11. Chronoamperometry of (a) the hybrid fuel cell and the enzymatic electrode at different hydrodynamic conditions for 30 min; (b) the hybrid fuel cell at 10 ml min^{-1} glucose flow rate for 24 h (exchange of the MEA denoted by a dashed line). Conditions: 5 mM glucose in 0.1 M phosphate buffer, pH 7.2, 37 °C, N_2 atmosphere; cathode 500 ml min^{-1} dry oxygen flow rate. Fuel cell has been polarized at 0.5 V and the enzymatic electrode at 0.05 V vs. SCE.

combination of these as well as some problems with the design of the fuel cell. According to the literature, a similar type of enzymatic anode shows very stable behavior during several days of operation [14], which corresponds to the observations in the present work. This makes anode deactivation, although possible, not likely. On the other hand, similar rate of fuel cell deactivation was reported by Fischback et al. [33], who observed pronounced current decay under constant operation. They were able to regain most of the initial performance by replacement of the MEA, which lead them to the conclusion that the loss of performance was due to poisoning of the membrane by cations from the anodic buffer solution [33]. Similar type of experiment with replacement of MEA was performed in this study and the results were in accordance to the latter work. As can be seen in Fig. 11b, the fuel cell restores activity almost to the initial level after exchange of the MEA, which is in accordance with the assumption that the enzymatic anode was not deactivated.

As discussed above, Fischback et al. assigned the fuel cell deactivation to impeded proton conductivity through the membrane caused by the competitive affinity of sodium or potassium cations to the anionic sulfonic sites of Nafion [33]. This phenomenon is expected to occur in the present case as well but according to our opinion it cannot explain such a high degree of performance loss. Okada et al. have shown that the ionic conductivity of Nafion decreases from ca. 0.2 to approximately 0.05 S cm^{-1}, when all protons are exchanged with alkali metal cations [45]. This change is not so dramatic and the membrane resistance itself (mΩ range) is expected to increase only about four times, which will lead to a negligible voltage drop, having in mind the low current densities (µA cm^{-2}) maintained by the fuel cell.

On the other hand, the exchange of protons with metal cations in the Nafion membrane, in addition to increase of the resistance, will lead to a significant change of pH at the cathode side, which will slow down the cathode kinetics. As discussed in the previous section, the pH difference between both electrodes is tentatively considered to be accountable for the demonstrated high OCV values. It can be envisaged that during long-term operation the overpotential at the cathode side will increase with pH increase. The stability test shown in Fig. 11b has been performed as a chronoamperometric experiment at 0.5 V (voltage, which corresponds to nearly maximum power as shown in Fig. 8). However, with the gradual neutralization of the cathode interface, the OCV of the system decreases and the value of 0.5 V (maintained by the potentiostat) does not correspond to the initial conditions anymore but is rather close to the newly formed OCV and consequently generates very low current densities. In addition, the 24 h test has been performed at higher glucose flow rate, which as shown in Fig. 11a, corresponds to higher rate of Nafion neutralization and glucose crossover, respectively.

This discussion compromises partly the use of the present fuel cell as a platform for investigation of enzymatic anodes under fuel cell conditions. However, as shown in Fig. 11a, the stability of the fuel cell at lower flow rates in the time scale, which corresponds to the typical duration of polarization curve recording, is satisfactory.

4. Conclusions

In the present study an enzymatic anode based on a charge-transfer complex (TTF–TCNQ) and glucose oxidase has been applied for the first time in a hybrid glucose–oxygen fuel cell. The CTC forms highly irregular porous structure, which serves a matrix for enzyme immobilization. This points out the importance of the enzyme distribution optimization within the catalyst layer. The optimized electrode reached high current densities and the fuel cell reached high power densities in presence of low glucose concentrations. The high OCV values demonstrated in the present study have been tentatively assigned to the different pH at both electrodes. This phenomenon has been accounted also for the lower long-term stability of the fuel cell. However, additional studies (e.g. with introduction of a reference electrode) are needed for unambiguous clarification of the high OCV and the mechanism of performance loss. The constructed device can be used as a platform for testing of enzymatic anodes but at lower glucose flow rates and shorter time scales.

Acknowledgments

The authors would like to thank Leonardo Sarmento and Torsten Schröder, who contributed to the design of the hybrid enzymatic fuel cell device and the fuel cell testing facility.

References

[1] I. Ivanov, T. Vidakovic-Koch, K. Sundmacher, Energies 3 (2010) 803–846.
[2] Y. Kamitaka, S. Tsujimura, N. Setoyama, T. Kajino, K. Kano, Phys. Chem. Chem. Phys. 9 (2007) 1793–1801.
[3] L. Stoica, N. Dimcheva, Y. Ackermann, K. Karnicka, D.A. Guschin, P.J. Kulesza, J. Rogalski, D. Haltrich, R. Ludwig, L. Gorton, W. Schuhmann, Fuel Cells 9 (2009) 53–62.
[4] N.L. Akers, C.M. Moore, S.D. Minteer, Electrochim. Acta 50 (2005) 2521–2525.
[5] R.L. Arechederra, S.D. Minteer, Fuel Cells 9 (2009) 63–69.
[6] A. Heller, Phys. Chem. Chem. Phys. 6 (2004) 209–216.

[7] S. Cosnier, D. Shan, S.N. Ding, Electrochem. Commun. 12 (2010) 266–269.
[8] E. Nazaruk, S. Smolinski, M. Swatko-Ossor, G. Ginalska, J. Fiedurek, J. Rogalski, R. Bilewicz, J. Power Sources 183 (2008) 533–538.
[9] G. Merle, A. Habrioux, K. Servat, M. Rolland, C. Innocent, K.B. Kokoh, S. Tingry, Electrochim. Acta 54 (2009) 2998–3003.
[10] N. Mano, F. Mao, A. Heller, J. Electroanal. Chem. 574 (2005) 347–357.
[11] F. Mao, N. Mano, A. Heller, J. Am. Chem. Soc. 125 (2003) 4951–4957.
[12] S.C. Barton, J. Gallaway, P. Atanassov, Chem. Rev. 104 (2004) 4867–4886.
[13] R. Pauliukaite, A. Malinauskas, G. Zhylyak, U.E. Spichiger-Keller, Electroanalysis 19 (2007) 2491–2498.
[14] G.F. Khan, M. Ohwa, W. Wernet, Anal. Chem. 68 (1996) 2939–2945.
[15] F. Palmisano, P.G. Zambonin, D. Centonze, M. Quinto, Anal. Chem. 74 (2002) 5913–5918.
[16] R. Pauliukaite, G. Zhylyak, D. Citterio, U.E. Spichiger-Keller, Anal. Bioanal. Chem. 386 (2006) 220–227.
[17] H.B. Liu, J.B. Li, C.S. Lao, C.S. Huang, Y.L. Li, Z.L. Wang, D.B. Zhu, Nanotechnology 18 (2007) 7.
[18] D. de Caro, K. Jacob, C. Faulmann, J.P. Legros, F. Senocq, J. Fraxedas, L. Valade, Synth. Met. 160 (2010) 1223–1227.
[19] J. Kulys, V. Simkeviciene, I.J. Higgins, Biosens. Bioelectron. 7 (1992) 495–501.
[20] H.J. Wang, J. Shi, M. Fang, Z. Li, Q.X. Guo, J. Phys. Org. Chem. 23 (2010) 75–83.
[21] N.S. Hudak, J.W. Gallaway, S.C. Barton, J. Electrochem. Soc. 156 (2009) B9–B15.
[22] A. Habrioux, K. Servat, S. Tingry, K.B. Kokoh, Electrochem. Commun. 11 (2009) 111–113.
[23] N.S. Hudak, S.C. Barton, J. Electrochem. Soc. 152 (2005) A876–A881.
[24] F. Tasca, L. Gorton, W. Harreither, D. Haltrich, R. Ludwig, G. Noll, J. Phys. Chem. C 112 (2008) 13668–13673.
[25] C.D. Jaeger, A.J. Bard, J. Am. Chem. Soc. 101 (1979) 1690–1699.
[26] M.T. Meredith, D.Y. Kao, D. Hickey, D.W. Schmidtke, D.T. Glat zhofer, J. Electrochem. Soc. 158 (2011) B166–B174.
[27] B. Kowalewska, P.J. Kulesza, Electroanalysis 21 (2009) 351–359.
[28] E. Nazaruk, K. Sadowska, J.F. Biernat, J. Rogalski, G. Ginalska, R. Bilewicz, Anal. Bioanal. Chem. 398 (2010) 1651–1660.
[29] S. Myler, S.D. Collyer, K.A. Bridge, S.P.J. Higson, Biosens. Bioelectron. 17 (2002) 35–43.
[30] P. Atanasov, A. Kaisheva, I. Iliev, V. Razumas, J. Kulys, Biosens. Bioelectron. 7 (1992) 361–365.
[31] H. Sakai, T. Nakagawa, Y. Tokita, T. Hatazawa, T. Ikeda, S. Tsujimura, K. Kano, Energy Environ. Sci. 2 (2009) 133–138.
[32] T. Reshetenko, H. Kim, H. Lee, M. Jang, H. Kweon, J. Power Sources 160 (2006) 925–932.
[33] M.B. Fischback, J.K. Youn, X.Y. Zhao, P. Wang, H.G. Park, H.N. Chang, J. Kim, S. Ha, Electroanalysis 18 (2006) 2016–2022.
[34] C.A. Apblett, D. Ingersoll, S. Sarangapani, M. Kelly, P. Atanassov, J. Electrochem. Soc. 157 (2010) B86–B89.
[35] V. Soukharev, N. Mano, A. Heller, J. Am. Chem. Soc. 126 (2004) 8368–8369.
[36] N. Mano, F. Mao, W. Shin, T. Chen, A. Heller, Chem. Commun. (2003) 518–519.
[37] R.A. Alberty, Biochem. Educ. 28 (2000) 12–17.
[38] H.F. Cui, J.S. Ye, W.D. Zhang, J. Wang, F.S. Sheu, J. Electroanal. Chem. 577 (2005) 295–302.
[39] A. Kongkanand, S. Kuwabata, G. Girishkumar, P. Kamat, Langmuir 22 (2006) 2392–2396.
[40] A. Parthasarthy, S. Srinivasan, A.J. Appleby, C.R. Martin, J. Electroanal. Chem. 339 (1992) 101–121.
[41] S.Z. Chen, F. Ye, W.M. Lin, Int. J. Hydrogen Energy 35 (2010) 8225–8233.
[42] T. Tamaki, T. Yamaguchi, Ind. Eng. Chem. Res. 45 (2006) 3050–3058.
[43] T. Kuwahara, K. Oshima, M. Shimomura, S. Miyauchi, J. Appl. Polym. Sci. 104 (2007) 2947–2953.
[44] N. Mano, Chem. Commun. (2008) 2221–2223.
[45] T. Okada, H. Satou, M. Okuno, M. Yuasa, J. Phys. Chem. B 106 (2002) 1267–1273.